International Journal of Science and Research (IJSR)
ISSN: 2319-7064
SJIF (2022): 7.942

Simulation of the Optical Properties of $Zn_{1-x}Co_xO$ Thin Films Grown Onto Glass Substrate by Ultrasonic Spray Pyrolysis

Sabrina. Roguai[1], Abdelkader Djelloul[2]

[1, 2]LASPI[2]A Laboratoire des Structures, Propriétés et Interactions Inter Atomiques, Université Abbes Laghrour, Khenchela 40000, Algérie

Email: *rog.sabrina[at]yahoo.fr*

Abstract: ***$Zn_{1-x}Co_xO$ thin films (x=0-22 at.%) were prepared using the ultrasonic pyrolysis sputtering technique. The films have a hexagonal wurtzite structure, confirmed by X-ray difraction, with an estimated average crystallite size in the range of 18-30 nm. Concerning the optical properties, by applying the Levenberg-Marquardt least squares method, the experimental transmittance data were perfectly fitted with the transmittance data calculated via a combination of the Wemple-DiDomenico model, the absorption coefficient of an electronic transition and the Tauc-Urbach model. Decreases in bandgap energy due to the presence of high concentrations of localized states in thin films were calculated from the Smakula formula***

Keywords: Thin films, X-ray diffraction, Optical properties

1. Introduction

Transparent Conductive Oxides (TCO) are remarkable materials in many fields. The existence of their dual properties, electrical conductivity and transparency in the visible range, makes them ideal candidates for applications in photovoltaics and optoelectronics. Zinc oxide ZnO is a semiconductor material belonging to this family of OCTs, it presents interesting electronic, electrical and optical properties for optoelectronic applications, especially in the photovoltaic field. The band gap is of direct nature, the value of its width varies from 3.3 eV to 3.4 eV and an excitonic binding energy of 60 meV [1]. The doping with cobalt is of great interest in many fields of application. Their particular properties make them suitable for use as optical components, integrated optical amplifiers,...

These films have been used in several electronic and optoelectronic fields such as: conductive gas sensors [2], light emitting diodes [3], photocatalytic reactors [4], optical windows in solar cells [5]. ZnO films can be made by several techniques such as: sputtering [6], chemical vapor deposition [7], sol gel and spray pyrolysis [8]. The aim of this work is to study the influence of Co-doping on the structural and optical properties of ZnO thi films.

2. Experimental Part

2.1 Film preparation

In this study, the ultrasonic pyrolysis spray technique was used to synthesize ZnO, $Zn_{1-x}Co_xO$ films. This technique is a relatively simple alternative that uses traditional and inexpensive means [9]. Its implementation is locally feasible. It also has the advantage of elaborating thin layers on large surfaces such as those of solar cells or flat screens [9,10]. From the advantages mentioned above, we have selected this elaboration process and we have opted for its use in our work. In fact 1.2g of zinc acetate [$C_4H_6O_4Zn.2H_2O$], We have as source material that we dissolved in50 ml of deionized water; 20 ml of CH3OH; 30 ml of C2H5OH. In addition to the undoped ZnO thin film, we prepared several series of layers, one of which is doped with Cobalt, 1-22% (Co, at. %) cobalt nitrate hexahydrate [Co $(NO_3)_2$-$6H_2O$] was used as the source of Co. To fix the pH value at about 4.8, a small amount of acetic acid was added, so as to prevent hydroxide evolution. The thin films were deposited on glass substrates (30 × 10 × 1.2 mm^3) at the temperature of 450 °C, weighting 30 min.

2.2 Characterization techniques

In order to study these parameters, different characterizations were performed. To do so, we characterized our films by X-ray diffraction in order to deduce the evolution of their microstructure by using a high resolution diffractometer (Rigaku Ultima IV powder) equipped with Cu-Kα radiation (λ=1.5418 Å). The optical properties were studied using UV-Visible transmission, with a Perkin Elmer UV-Vis-NIR spectrophotometer (Lambda 19) in the range 190-1800 nm.

3. Results and discussion

3.1 Structure analysis

The X-ray diffraction spectra show the presence of the wertzite phase of the hexagonal structure of ZnO according with (JCPDS card no. #00–036–1451) [10]. Deposits obtained with Co concentrations show a strong preferential orientation along the (002) axis in the set of films, without any other impurity phase at least within the detection limits of X-ray diffraction. This result clearly indicates that Co^{2+} can be incorporated into the ZnO lattice developed by Ultrasonic Spray method without any phase segregation taking place in these films. We also observe an increase in peak intensity as a function of doping rate. The results of the phases examined qualitatively and quantitatively by the Rietveld method are shown in Table 1.The value of the lattice parameter "a" rises with increasing Co content, while

the value "c" seems to be little influenced. The values of crystallite size changes in a small range of 18-30 nm, while the micro-strain considerably varies with the Co content in the range of 0.131-0.289%.

Table 1: X-ray diffraction Rietveld refinements results

Composition	Crystallite size (nm)	Microstrain (%)	Lattice parameters (Å)	
ZnO	25	0.266	a=3.2542	c=5.2129
$Zn_{0.99}Co_{0.01}O$	21	0.096	a=3.2577	c=5.2124
$Zn_{0.97}Co_{0.03}O$	35	0.230	a=3.2594	c=5.2172
$Zn_{0.95}Co_{0.05}O$	23	0.289	a=3.2572	c=5.2162
$Zn_{0.91}Co_{0.09}O$	22	0.131	a=3.2613	c=5.2172
$Zn_{0.86}Co_{0.14}O$	25	0.143	a=3.2605	c=5.2148
$Zn_{0.82}Co_{0.18}O$	18	0.147	a=3.2689	c=5.2230
$Zn_{0.78}Co_{0.22}O$	18	0.142	a=3.2644	c=5.2167

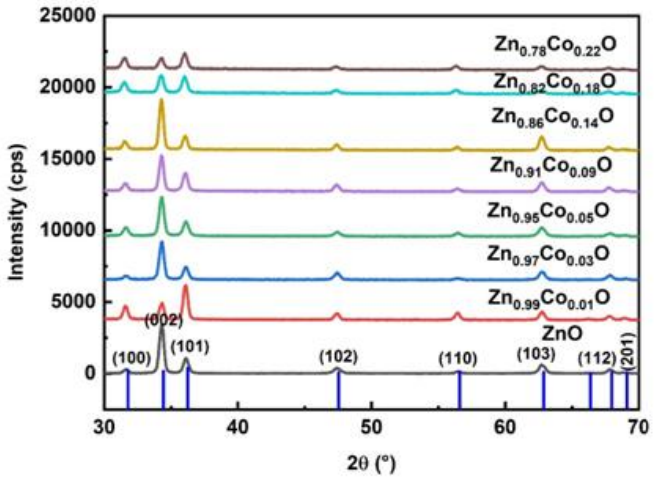

Figure 1: XRD patterns of pure ZnO and Co-doped ZnO films

For a semiconductor with a wide band gap with a magnetic impurity, to have dilute magnetic semiconductor (DMS) applications, the impurity must be uniformly distributed to achieve the inherent ferromagnetism in the system. When Co^{2+} ions are substituted in Zn^{2+} sites, they do not contribute to the charge density. However, the Co^{2+} ion has seven electrons in the 3d state. The odd number of electrons in the outermost layer (the 3d sublayer) produces magnetic moments with spin-orbit coupling. When an atom has several electrons, its magnetic moment $\vec{M}$ is associated with the total angular momentum $\vec{L}$, which is the sum of the orbital magnetic moment $-g_L\mu_B\vec{L}$ and the spin magnetic moment $-g_S\mu_B\vec{S}$:

$$M = -g\mu_B\vec{J} \qquad \text{and,} \qquad \mu_{eff} - g\mu_B\sqrt{J(J+1)}$$

where g is the Landé factor expressed as a function of the principal quantum numbers (S, L, J). is the effective magnetic moment per atom. The value of the saturation magnetization of the material ($M_S = g'\mu_B V/N$) will depend on the Landé factor.

$$g_J = g_L\frac{J(J+1)-S(S+1)+L(L+1)}{2J(J+1)} + g_S\frac{J(J+1)+S(S+1)-L(L+1)}{2J(J+1)} \quad (1)$$

is approximately

$$g_J \approx 1 + \frac{J(J+1)-L(L+1)+S(S+1)}{2J(J+1)} \quad (2)$$

With $g_L \approx 1; \quad g_S \approx 2$

The calculation of the spin S involves only the valence electrons.In a first approximation, the magnetic moments carried by the transition metal atoms inserted in ZnO are pure spin moments, integer numbers of μ_B, $\mu_B = q\hbar/2m_e$ the Bohr magneton (q being the charge of the electron, me the mass of the electron and the reduced Planck constant).

Thus we can calculate the theoretical value of the magnetic moment carried by each transition metal atom according to its electronic structure.

In the case of Co(II) orbital magnetic moment is frozen and therefore considered as zero for the 3d electrons, because the spin-orbit interaction becomes negligible in front of the crystal field of the neighboring ions, because contrary to the 4f electrons in the case of rare earths, which are on deep levels, they are not screened by the electrons of external layers.

For an atom, the Landé factor is used to calculate the atomic energy levels in a weak magnetic field. If we are interested in the electronic angular momentum J, sum of the electronic spin S and the orbital angular momentum L, the Landé factor is :

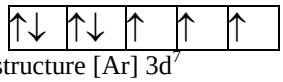

Co^{2+}: electronic structure [Ar] $3d^7$

This configuration corresponds to 3 unpaired electrons, a spin magnetic moment and thus a Co moment. In Table 2.

Table 2: Experimental and theoretical magnetic moment values (μ_{eff}) as a function of the transition metal. 3d ions, μeff is in unit μ_B/atom [11]

$3d^n$	Transition metal	Fundamel state	S	L	J	g	μ_{eff} $g\sqrt{J(J+1)}$	μ_{eff} $g\sqrt{S(S+1)}$	μ_{eff}^{exp}
1	Ti^{3+}, V^{4+}	$^2D_{3/2}$	1/2	2	3/2	4/5	1.55	1.73	1.7
2	Ti^{2+}, V^{3+}	$^3F_2$	1	3	2	2/3	1.63	2.83	2.8
3	V^{2+}, Cr^{3+}	$^4F_{3/2}$	3/2	3	3/2	2/5	0.78	3.87	3.8
4	Cr^{2+}, Mn^{3+}	$^5D_0$	2	2	0	/	/	4.90	4.9
5	Mn^{2+}, Fe^{3+}	$^6S_{5/2}$	5/2	0	5/2	2	5.92	5.92	5.9
6	Fe^{2+}, Co^{3+}	$^5D_4$	2	2	4	3/2	6.71	4.90	5.4
7	Co^{2+}, Ni^{3+}	$^4F_{9/2}$	3/2	3	9/2	4/3	6.63	3.87	4.8
8	Ni^{2+}	$^3F_4$	1	3	4	5/4	5.59	2.83	3.2
9	Cu^{2+}	$^2D_{5/2}$	1/2	2	5/2	6/5	3.55	1.73	1.9

It appears that the magnetism of the 3d series is due to the spin moment, with little or no orbital contribution. S is the correct quantum number for the 3d series. An exception seems to be Co^{2+}, where an orbital contribution increases μ_{eff} significantly above the spin-only value.

The magnetic moment of bulk cobalt is 1.85 μ_B (μ_B: Bohr magneton)[12]. When the distance between Co ions is close enough, the inherent ferromagnetism can be induced by a direct exchange interaction between the magnetic dipoles of Co ions. As there is a spin-orbit coupling, there is also a spin-spin coupling named Heisenberg exchange interaction. The interaction responsible for the alignment of the spins is generally called exchange interaction.

The coupling between the spins of two electrons belonging to neighboring atoms (i and j) has an energy of the form $-J_{ex}(\vec{S}_i.\vec{S}_j)$ (J_{ex}, measure of the spacing of spin excitations). This energy results from the Coulomb interelectronic interactions and the Pauli exclusion principle of the spins $\vec{S}_i$ and $\vec{S}_j$. The sign of the exchange integral (in J) defines the orientation of the spins $\vec{S_i}$ and $\vec{S_j}$:

- antiferromagnetic order for Jex<0 : the spins are oriented in opposite directions.
- ferromagnetic order for Jex>0 : the spins are oriented in the same direction.

The link between the exchange integral and the Landau exchange constant A (in J/m) is written :

$$A = \frac{\mu_{0M_S^2}}{2}\left(\frac{2J_{ex}S(S+1)}{\mu_{0M_S^2}}\right)^{2/3} \quad (3)$$

The exchange integral of pure cobalt is $=2.2\times10^{-21}$ J (~14 meV) [13]. μ_0 (magnetic permeability of vacuum)= $4\pi\times10^{-7}$ T.m/A. The spin value S for cobalt and cobalt-based alloys is 3/2 and the saturation magnetization of cobalt Ms=1.42×10^6 A/m [14]. Exchange coupling is a short-range interaction because the value of the exchange constant depends on the overlap of the atomic orbitals. The range over which this energy couples neighboring magnetic moments is defined by the exchange length : $\delta_{ex} = \sqrt{2A/\mu_0 M_s^2}$, or ≈ 1.8 nm for cobalt-based thin films.

For uniformly distributed Co ions, the average distance between Co ions that have been substituted in Zn sites of ZnO can be evaluated via a simple calculation

$$\Delta V/\Delta N \approx 4\pi R^2(dR/dN)\ ,\ N = (\Delta N/\Delta V)\times(4/3)\pi R^3 \quad (4)$$

where R is the average radius of an atomic sphere and N is the number of atoms in the sphere. For zinc atoms in the wurtzite structure of ZnO, $\Delta N/\Delta V \approx 42.1 nm^{-3}$.

Figure.2. represents the number of zinc atoms in a sphere of radius R. In the $Zn_{0.97}Co_{0.03}O$ film, 3% of the zinc sites are occupied by cobalt ions. Therefore, the 33rd zinc site from the probed atom is occupied by cobalt. The calculated average distance between the cobalt ions is estimated to be about 0.574 nm, which means that the closest Co ion to a probed Co ion is located in the next cell. In the $Zn_{0.95}Co_{0.05}O$ film, the average distance of Co-Co pairs is about 0.484 nm. In the $Zn_{0.91}Co_{0.09}O$ film, the average Co-Co pair distance is about 0.398 nm. A theoretical calculation shows that the exchange interaction between the magnetic ions has not disappeared in less than a multiple of 1.5 of a lattice constant [15]. The calculation shows that 3% doping is the minimum amount for the inherent ferromagnetism in ZnCoO to be induced by the exchange interaction between magnetic ions without charge mediation. This study demonstrates that the ferromagnetic properties of ZnCoO with Co concentrations above 3% can be inherent since the Co ions uniformly occupy the zinc sites.

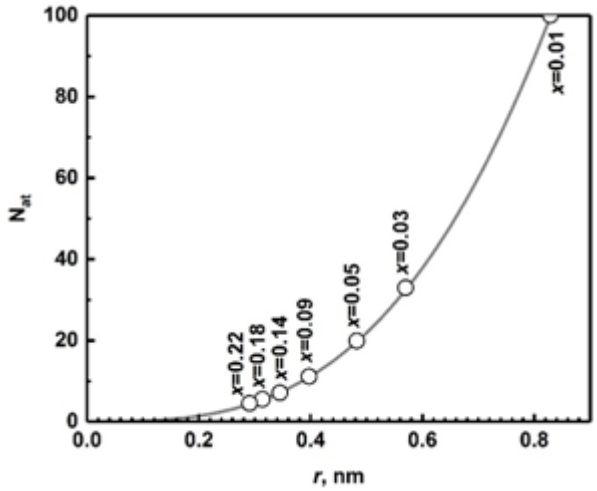

Figure 2: Number of zinc atoms in a sphere with a radius of r for wurtzite ZnO

3.2 Optical analysis

Figures .3. show that the UV/visible spectra of the ZnO, $Zn_{1-x}Co_xO$ layers (x=0.01- 0.22). Localized absorption peaks at 657, 610 and 567 nm for all layers can be assigned to $^4A_2(F) \rightarrow {}^2E(G)$, $^4A_2(F) \rightarrow {}^4T_1(P)$ and $^4A_2(F) \rightarrow {}^4A_1(G)$ of Co^{2+} and are attributed to the transitions, crystal fields, in the high spin state of Co^{2+} in the tetrahedral coordination, suggesting that tetrahedrally coordinated Co^{2+} ions substitute Zn^{2+} ions in the hexagonal wurtzite structure [16]. Between 1272 and 1647 nm an additional transition, crystal field, was observed, named $^4A_2(F) \rightarrow {}^4T_1(F)$.

The solid curve in Fig. 3. correspond to the fitted curve using and the closed circle represents the experimental data[17]. The figures reveal a reasonable good fit to the experimental data, which implies an accurate determination of the parameters. The values of d, Eg, E_d, E_0, and n at 598 extracted by fitting the experimental results are listed in Table 3.

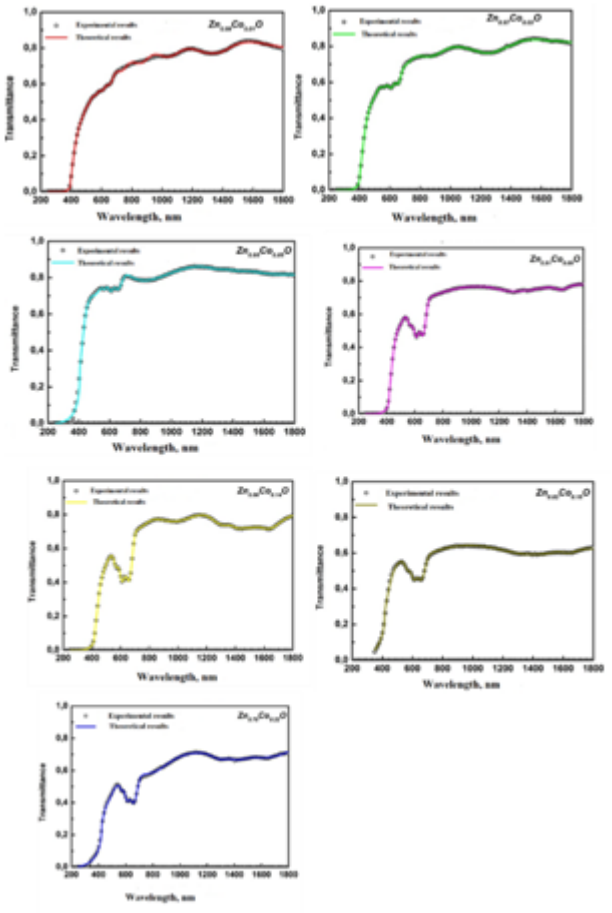

Figure. 3. Transmission spectra of pure ZnO and Co-doped ZnO thin flms deposited on glass substrate at 450 °C. Measured (full circles) and calculated (solid lines) transmittance spectra of flms.

Table 3: Dispersion parameters of the films

	Thickness, nm	E_g, eV	E_d, eV	E_0, eV	*n* at 598 nm
ZnO	486	3.258	11.334	6.018	1.771
$Zn_{0.99}Co_{0.01}O$	1382	3.133	11.318	6.199	1.749
$Zn_{0.97}Co_{0.03}O$	910	3.073	10.821	6.199	1.722
$Zn_{0.95}Co_{0.05}O$	343	3.045	12.372	5.820	1.854
$Zn_{0.91}Co_{0.09}O$	280	2.971	09.929	6.199	1.677
$Zn_{0.86}Co_{0.14}O$	733	2.946	09.396	5.393	1.745
$Zn_{0.82}Co_{0.18}O$	250	2.983	10.242	5.390	1.801
$Zn_{0.78}Co_{0.22}O$	597	2.928	09.076	5.393	1.727

In the ultrasonic pyrolytic spray deposition method, the film growth is achieved by thermal decomposition of a precipitate at the substrate; this deposition results from the vaporization of aerosol droplets. In this situation, the material that is formed contains different types of defects leading to a disorder in the structure. In this case, the band edges of the crystal lattice bounded by E_V and E_C may disappear. So-called localized states in the band gap are observed, which appear as band tails at the borders of the valence and conduction bands. For energies higher than EC and lower than EV, we find the extended states. When the disorder becomes too important (for example with the appearance of dangling bonds or impurities in the material), the tails can overlap. We then define the notion of Urbach parameter (E_{Urb}) to characterize this disorder. It is possible to estimate the disorder existing in the layers by studying the variations of the absorption coefficient. Indeed, the absorption coefficient can be expressed by the relation [18]

$$\alpha = \alpha_0 exp\left(\frac{h\nu}{E_{Urb}}\right), h\nu < E_g \quad (5)$$

E_{Urb} (=E_0) measures the extension of the Urbach tail and is an indirect measure of structural disorder and can be evaluated as the width of the localized state. Srikant et al [19] interpreted the Urbach energy EUrb as the bandwidth of localized states within the bandgap width. Figure 4. (lnα versus energy) shows the regions where different types of optical absorption phenomena occur: (1) exciton absorption, (2) fundamental absorption (valence band to conduction band transition and Urbach tail) and (3) impurity absorption.

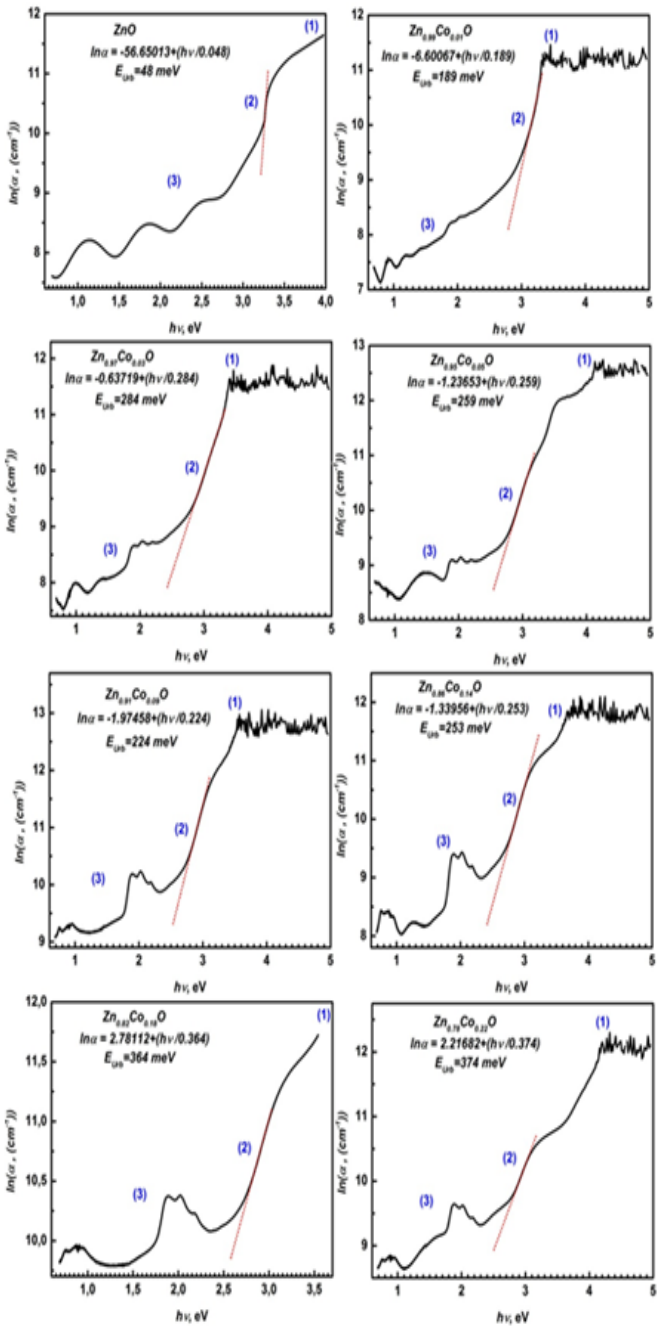

Figure 4: Evolution of the disorder (Urbach tail) as a function of the cobalt content

The E_{Urb} parameter is the band tail width which characterizes the disorder, and is comparable to that found by Srikant et al [19], and lies between 77 and 100 meV for ZnO. Values of about 48-374 meV for E_{Urb} can be deduced from our measurements (Figure 4.). This energy is about 30 meV [18] for single crystal ZnO (after annealing in air). Since this parameter is related to the disorder in the material, this indicates that our ZnO deposit is low in disorder compared to the single crystal in contrast to the $Zn_{1-x}Co_xO$ thin films which are highly disordere

4. Conclusion

ZnCoO thin films with different initial Cobalt concentrations ranging from 1 to 22%at were prepared by the ultrasonic pyrolytic sputtering technique deposited on glass substrates. X-ray diffraction analysis of the developed undoped and Co-doped samples shows that the thin films crystallize in the hexagonal Wurtzite-like structure. We noticed that the lattice parameters increase to reach (a = 3.2689 Å and c = 5.2230 Å) for a doping rate of 18 %at. The evolution of the lattice parameters with Co content is more complex than expected. The XRD analysis indicates that both undoped and doped ZnO thin films showed a preferential orientation along the c-axis perpendicular to the substrate surface. The average crystallite size decreases with Co insertion, which follows the decrease in the ionic radius of Co^{2+} compared to Zn^{2+}. A part of Co thus seems to be well inserted in substitutional position of Zn. On the other hand, for $Zn_{0.97}Co_{0.03}O$ this tendency does not apply and for $Zn_{0.86}Co_{0.14}O$ the same crystallite size as ZnO was found UV-vis spectroscopy results show a red shift in the gap and an increase in the intensity of Co absorption peaks as the Co concentration increases. The reproduced transmittance curve using the fitting parameters d, n and k, is in good agreement with the experimental transmittance data.

Acknowledgements
Funding was provided by the General Direction of research and development technologies/ Ministry of Higher Education and Research Sciences DGRSDT/ MESRS, Algeria. The financial support from Abbes Laghrour University of Khenchela (Algeria). The authors would like to thank the National Project Research (PNR) and LASPI^{2}A Laboratory of Khenchela University (Algeria) for their financial support of this research project. The authors thank Pr. Abdecharif Boumaza for FTIR analysis, Laboratoire des Structures, Propriétés et Interactions Inter Atomiques (LASPI2A), Université Abbes Laghrour, 40000 Khenchela, Algeria.

References

[1] S. Benramache, B. Benhaoua, Superlattices and Microstructures. 52 (2012) 807-815.
[2] S. Wei, J. Lian, H. Wu, Materials Characterization. 61 (2010) 1239 – 1244.
[3] L. Castaneda, A. Maldonado, A.E. Morales et al. Materials Science in Semiconductor Processing. 14 (2011) 114–119.
[4] B.N. Pawar, S.R. Jadkar, M.G. Takwale, Journal of Physics and Chemistry of Solids. 66 (2005) 1779–1782.
[5] S. Rani, P. Suri, P.K. Shishodia, R.M. Mehra, Solar Energy Materials & Solar Cells. 92 (2008) 1639–1645.
[6] Z. Ben Ayadi, L. El Mir, K. Djessas, S. Alaya, Thin Solid Films. 517 (2009) 6305– 6309.
[7] H. Kavak, E. S. Tuzemen, L.N. Ozbayraktar, R. Esen, Vacuum. 83 (2009) 540–543.
[8] S. Ilican, Y. Caglar, M. Caglar, F. Yakuphanoglu, Applied Surface Science. 255 (2008) 2353–2359
[9] S. Roguai, A.Djelloul, Applied Physics A.126 (2020) 122
[10] S. Roguai, A.Djelloul, Reaction Kinetics, Mechanisms and Catalysis. (2021).//doi.org/10.1007/s11144-021-01963-4
[11] K.J.H.Buschow, F.R.de Boer, Physics of Magnetism and Magnetic Materials, Kluwer Academic Publishers New York,Boston, Dordretcht, London, Moscow, 2004
[12] Springer-Verlag, editor. Magnetic properties of metals, volume 19. Landolt-Börnstein, 1986.
[13] S. Uchiyama, Materials chemistry and physics, 42 (1995) 38-44.
[14] J. A. Katine, F. J. Albert, R. A. Buhrman, E. B. Myers, and D.C. Ralph, Phys. Rev. Lett. 84 (2010) 3149.
[15] L. Bergqvist, O. Eriksson, J. Kudrnovsky, V. Drchal, P. Korzhavyi, L. Turek, Physical Review Letters 93 (2004) 137202.
[16] H.A. Weaklim, J.Chem.Physi.36 (1962) 2117-2140
[17] S. Roguai, A. Djelloul, C. Nouveau, T. Souier, A. A. Dakhel, M. Bououdina, J. Alloys Compd. 599 (2014) 150–158.
[18] J.I. Pankove, Optical Processes in Semiconductor, Prentice-Hall, New Jersey,1971.
[19] V. Srikant, D.R.Clarke ,J.Appl.Phys.81 (1997) 6357.